한국윤활학회지(1996), 제12권 제2호
Journal of KSTLE(1996) Vol. 12, No. 2, pp.41~47

A Design of Self-Acting Air Lubricated Spindle

Museok Song, Dong-Seob Jang* and Young-Ze Lee**

Department of Naval Architecture and Ocean Engineering, Hong Ik University
**R&D Center, Samsung Electro-Mechanics Co.*
***School of Mechanical Engineering, Sung Kyun Kwan University*

공기동압 스핀들의 설계

송무석 · 장동섭* · 이영제**

홍익대학교 조선해양공학과, *삼성전기(주) 종합연구소
**성균관대학교 기계공학부

초 록—고속에서 작동하는 공기동압 스핀들을 개발하기 위해 축방향 하중을 포함하여 설계와 관련된 문제들을 살펴보았다. 협곡이론에 근거한 지배방정식을 사용하였고, 차분법을 사용하여 해석하였다. 설계인자인 홈의 형상, 홈의 각도, 회전수, 그리고 편심량 등을 사용하여 축방향과 원주방향의 압력분포를 수치해석적으로 구하였다.

1. Introduction

Recently, machinery equipped with high speed rotating parts have been widely used even in everyday life. Moreover, for better performance of such machinery, the demand for even higher rotating speed is increasing. For bearings used in such parts usually require relatively clean environment, and, for this reason, conventional oil based lubrications can hardly applicable due to its evaporating or spattering characteristics. One solution for such problems is introducing hydrodynamic bearings using air as lubricating fluid. Various types of hydrodynamic bearing spindles have been studied by numerous researchers [1-3] and one of them is spindles with grooves of oblique angle. In order to design such type of rotor/spindle set, rotating at 7200 RPM and supporting 300g mass, we performed a numerical investigation with varying various controlling parameters. Based on the preliminary results, we designed and manufactured a prototype rotor/spindle set and the validating experiment is underway.

Here we briefly explain the numerical procedure, discuss related matters based on the results basically for the proposed bearing shape and summarize at the end.

2. Formulation of the Problem

The governing equation for the flow in lubricating films can be solved by various numerical methods under appropriate assumptions [4-6]. Among them, for the cases in which relatively dense grooves are used, the well known narrow groove theory is believed to provide reliable information about the pressure [3,7-10]. Since our principal goal is to obtain a preliminary pressure information which is generated by the air flow associated with sleeve rotation around a narrowly grooved spindle, we simply adopted the narrow groove theory here. Hence, the formulation of the problem is given very briefly here without detail (see [7]).

The coordinate system and the control volume used in the formulation are shown in Fig. 1. The control volume is bounded by the upper and lower surfaces moving at $w_2 r$ and $w_1 r$, respectively.

Defining ψ_s and ψ_θ as stream functions in s- and θ-direction, respectively and applying the mass conservation to the control volume shown in Fig. 1 gives

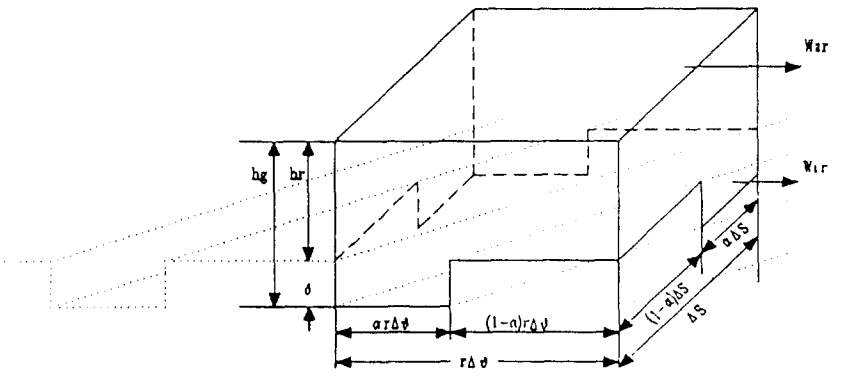

Fig. 1. Definition sketch. α is the groove ratio.

$$\triangle s\frac{\partial}{\partial s}(\triangle\psi_s)+\triangle\theta\frac{\partial}{\partial\theta}(\triangle\psi_\theta)+\frac{\partial}{\partial t}[\alpha h_g+(1-\alpha)h_r]\rho r\triangle\theta\triangle s=0 \tag{1}$$

Here, subscript g and r indicates that the variable is for groove and ridge, respectively.

The mass flux vector for an isothermal film [11] is

$$\Psi=\rho\int_0^h \underline{v}\,dz=-\frac{\rho h^3}{12\mu}\nabla p+\frac{\rho h}{2}\underline{U} \tag{2}$$

or in component form with noting $\underline{U}=\frac{w_1+w_2}{2}r\rho h$,

$$\psi_\theta=-\frac{\rho h^3}{12\mu}\left(\frac{1}{r}\frac{\partial p}{\partial\theta}\right)+\frac{w_1+w_2}{2}r\rho h$$

$$\text{and } \psi_s=-\frac{\rho h^3}{12\mu}\left(\frac{\partial p}{\partial s}\right) \tag{3}$$

The flux normal to groove can be written as

$$\psi_n=\psi_\theta\sin\beta-\psi_s\cos\beta$$

$$=\left(-\frac{\rho h^3}{12\mu_g r}\frac{\partial p}{\partial\theta}+\frac{w_1+w_2}{2}r\rho h\right)\sin\beta+\frac{\rho h^3}{12\mu_s}\frac{\partial p}{\partial s}\cos\beta, \tag{4}$$

where β is the groove angle, and applying flux continuity along the groove/ridge boundary we have the following relation.

$$\psi_{ng}=\psi_{nr}+w_1 r\rho\delta\sin\beta. \tag{5}$$

Inserting the equation (4) into the equation (5) gives a partial differential equation for the pressure.

Assuming the groove size is small and using pressure continuity, pressure gradient in each direction can be represented in terms of so called "macroscopic pressure" which is an "averaged" pressure over one segment of groove ridge cell given in Fig. 1. Then the mass fluxes are expressed in terms of this macroscopic pressure and substituting these fluxes into the equation (1) gives

$$\frac{1}{r}\frac{\partial}{\partial s}\left[\rho h_r^3\left(K_1 r\frac{\partial p'}{\partial s}+K_2\frac{\partial p'}{\partial\theta}\right)-\rho r^2K_\delta K_4^s\cos\beta\right]+\frac{1}{r^2}\frac{\partial}{\partial\theta}\left[\rho h_r^3\left(K_2 r\frac{\partial p'}{\partial s}+K_3\frac{\partial p'}{\partial\theta}\right)+\rho r^2K_\delta K_4^\theta\sin\beta\right]$$

$$-6\mu_a(w_1+w_2)\left[\frac{\partial}{\partial\theta}+\frac{2}{w_1+w_2}\frac{\partial}{\partial t}\right](\rho h_r K_w)=0 \tag{6}$$

where, $K_1=\dfrac{K_s K_\theta\alpha(1-\alpha)\sin^2\beta+\Gamma^3[(1-\alpha)K_{gg}/\bar{\mu}_r+\alpha K_{rr}/\bar{\mu}_g]}{(1-\alpha)\Gamma^3K_{gg}+\alpha K_{rr}}$,

$K_2=\dfrac{K_s K_\theta\alpha(1-\alpha)\cos\beta\sin\beta}{(1-\alpha)\Gamma^3K_{gg}+\alpha K_{rr}}$,

$K_3=\dfrac{K_s K_\theta\alpha(1-\alpha)\cos^2\beta+\Gamma^3[(1-\alpha)K_{gg}/\bar{\mu}_r+\alpha K_{rr}/\bar{\mu}_g]}{(1-\alpha)\Gamma^3K_{gg}+\alpha K_{rr}}$,

$$K_s=\frac{\Gamma^3}{\bar{\mu}_g}-\frac{1}{\bar{\mu}_r},\quad K_\theta=\frac{\Gamma^3}{\bar{\mu}_g}-\frac{1}{\bar{\mu}_r},\quad K_{gg}=\frac{\cos^2\beta}{\bar{\mu}_g}+\frac{\sin^2\beta}{\bar{\mu}_g},$$

$$K_{rr}=\frac{\cos^2\beta}{\bar{\mu}_r}+\frac{\sin^2\beta}{\bar{\mu}_r},\quad K_4^s=\frac{K_s}{(1-\alpha)\Gamma^3K_{gg}+\alpha K_{rr}},$$

$$K_4^\theta=\frac{K_\theta}{(1-\alpha)\Gamma^3K_{gg}+\alpha K_{rr}},\quad K_\delta=6\mu_a(w_2-w_1)\alpha(1-\alpha)\delta\sin\beta,$$

$$K_w=\alpha\Gamma+(1-\alpha),\Gamma=\frac{h_g}{h_r},\bar{\mu}_g=\frac{\mu_g}{\mu_a},\bar{\mu}_r=\frac{\mu_r}{\mu_a}\text{ and }\mu_g=\frac{\mu_a}{1+\frac{6\lambda_a p_a}{ph_g}},\ \mu_r=\frac{\mu_a}{1+\frac{6\lambda_a p_a}{ph_r}}.$$

Although if turbulent flow is expected some correction is usually required, the Reynolds number based on the clearance in our case is low enough not to include such effects. Dimensionless form of the above equation is the following final expression which is used for the calculation.

$$\frac{1}{R}\frac{\partial}{\partial S}\left[\bar{\rho}H_r^3\left(K_1R\frac{\partial P}{\partial S}+K_2\frac{\partial P}{\partial\theta}\right)-\bar{\rho}R^2\Lambda_\delta K_4^s\cos\beta\right]$$
$$+\frac{1}{R^2}\frac{\partial}{\partial\theta}\left[\bar{\rho}H_r^3\left(K_2R\frac{\partial P}{\partial S}+K_3\frac{\partial P}{\partial\theta}\right)+\bar{\rho}R^2\Lambda_\delta K_4^\theta\sin\beta\right]-\Lambda\left[\frac{\partial}{\partial\theta}+\frac{2w_2}{w_1+w_2}\frac{\partial}{\partial T}\right](K_w\bar{\rho}H_r)=0 \tag{7}$$

where, $P=p/p_a$, $H_r=h_r/C$, $\bar{\rho}=P$, $S=s/R_o$, $R=r/R_o$, $T=w_2t$,

$$\Lambda=\frac{6\mu_a(w_2+w_1)}{p_a}\left(\frac{R_o}{C}\right)^2\text{and }\Lambda_\delta=\frac{6\mu_a(w_2-w_1)}{p_a}\left(\frac{R_o}{C}\right)^2\left(\frac{\delta}{C}\right)\alpha(1-\alpha)\sin\beta.$$

Here, C is the nominal gap.

3. Numerical Methods

If there is no eccentricity, the problem turns out to be axisymmetric and the equation (7) becomes the following form.

$$\frac{\partial}{\partial S}\left[PK_1\frac{\partial P}{\partial S}-P\Lambda_\delta K_4^s\cos\beta\right]-2\Lambda\frac{\partial}{\partial T}(K_wP)=0 \tag{8}$$

where the coefficients in the equation are explained in the previous section.

By using the central differencing and introducing a relaxation parameter (γ, [12]), the equation (8) can be discretized as follows;

$$\frac{1}{\triangle T}\left\{(K_w)_i^nP_i^{n+1}-(K_w)_i^nP_i^n\right\}$$
$$=\frac{\gamma}{2\Lambda}\left[\frac{\partial}{\partial S}(K_1P\frac{\partial P}{\partial s})_i^{n+1}-\frac{\partial}{\partial S}(\Lambda_\delta K_4^s\cos\beta)_i^{n+1}\right]+\frac{1-\gamma}{2\Lambda}\left[\frac{\partial}{\partial S}(K_1P\frac{\partial P}{\partial s})_i^n-\frac{\partial}{\partial S}(\Lambda_\delta K_4^s\cos\beta)_i^n\right]$$
$$=\frac{1-\gamma}{2\Lambda\triangle S^2}\left[P_{i+1}^n\frac{(K_1P)_i^n+(K_1P)_{i+1}^n}{2}-P_i^n\frac{(K_1P)_{i-1}^n+2(K_1P)_i^n+(K_1P)_{i-1}^n}{2}P_{i-1}^n\frac{(K_1P)_i^n+(K_1P)_{i-1}^n}{2}\right]$$
$$-\frac{1-\gamma}{4\Lambda\triangle S}\left[(\Lambda_\delta K_4^s\cos\beta)_{i+1}^nP_{i+1}^n-(\Lambda_\delta K_4^s\cos\beta)_{i-1}^nP_{i-1}^n\right]. \tag{9}$$

In the equation (9), in order to make the matrix for P_i^{n+1} tridiagonal, a linear interpolation is used for the first derivatives of nonlinear terms, and the coefficients are estimated at the old time (n-th time step). For the relaxation parameter, 0.7 is used after several trials, and the time integration is continued until

$\sum|P_i^{n+1}-P_i^n|$ becomes small enough. As boundary conditions, the atmospheric pressure is given at the bearing bottom and the zero pressure gradient is used at the top.

In order to take account for the effect of eccentricity we need to solve the full equation (7), and that two-dimensional equation is also solved by using a similar standard finite difference method (ADI method, [12]). A relaxation parameter is also used and the same boundary conditions as the axisymmetric case are applied.

4. Results and Discussions

Based on the operation requirement and the results from preliminary calculations primary shape of the spindle is determined as shown in Fig. 2. The diameter is 13 mm and 4 sets of grooved section with different groove angle are placed. There are 8 groove/ridge sets along the circumference. The groove ratio is fixed at 0.5 and the groove depth is 0.5 micron. The first grooved section from the bottom plays the role to generate air flow upward and sections with grooves of opposite direction make the flow downward. We can easily expect there will be two pressure peaks along the meridian and these two peaks stabilize the rotating sleeve's lateral motion. As we notice, the total upward flow section length is larger than that of downward flow section and this arrangement provide us with a certain amount of lifting force at the top.

In this section we confine our discussion to the given geometry unless otherwise stated and the discussion is divided into two subsections for one-dimensional and two-dimensional cases.

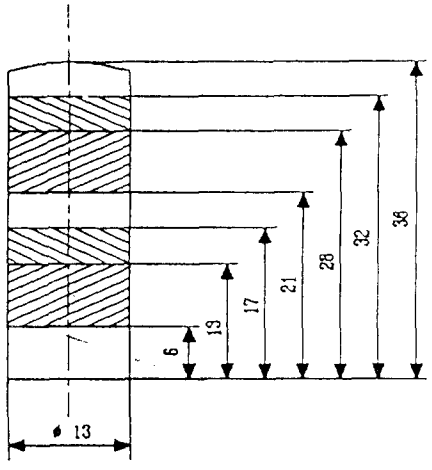

Fig. 2. Spindle geometry. Unit is mm.

4-1. Axisymmetric Cases

Fig. 3 shows the convergence characteristics during the calculation for groove angle β=25 deg and this trend is typical. The error remains constant in the mean which is in the round off error range after a certain amount of dimensionless time and then we can take the result as steady solution.

In order to investigate the effect of groove angle the angle has been varied from 15° to 35° and the results are summarized in Fig. 4 and 5. The RPM is fixed at 7200. When the clearance is 3 micron, basically very similar pressure distribution is obtained in all cases except that the peak values and the pressure at the top (the right end in the Fig) are changed a little according to the angle variation. As we expected, two pressure peaks are clearly shown and a

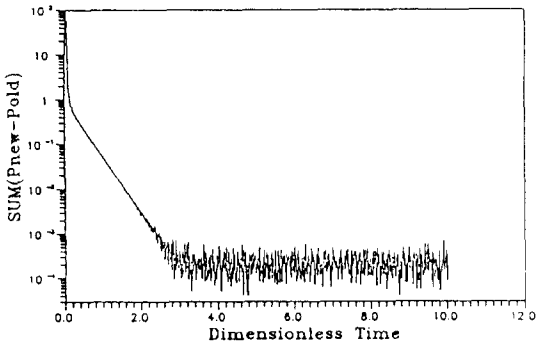

Fig. 3. A typical convergence characteristics of axisymmetric calculation.

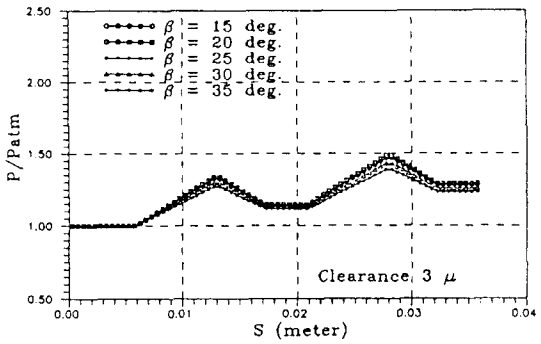

Fig. 4. Pressure distribution along a meridian for various groove angles. Clearance is 3 micron. Groove array is given in Fig. 2.

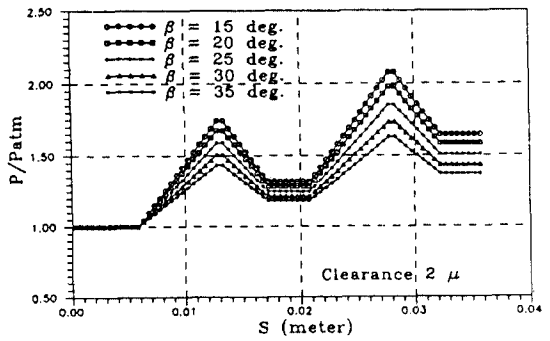

Fig. 5. Pressure distribution along a meridian for various groove angles. Clearance is 2 micron. Groove array is given in Fig. 2.

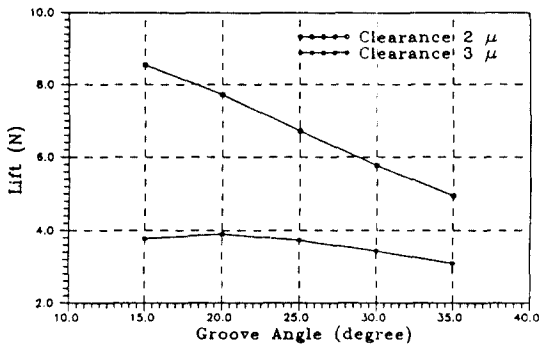

Fig. 6. Lift as a function of groove angle.

considerable amount of lifting pressure is generated at the top in all cases. Fig. 5 is for 2 micron clearance. Basically similar results obtained as for 3 micron clearance case and the effect of groove angle looks more prominent. Comparing the cases of 2 and 3 micron clearance we notice a significant pressure difference especially at the peaks. From this we can have a rough idea that this type of bearing might produce a considerable amount of lateral restoring force which in turn provides a sufficient bearing stiffness.

The lift force is summarized as a function of groove angle in Fig. 6. For the lift force estimation, the pressure at the top is assumed constant over the circle. Generally speaking smaller groove angles are more effective in terms of larger lift. However, this statement is not always correct as we notice that the maximum lift is obtained at 20° for 3 micron clearance case. If the assembled rotating sleeve weighs 300 g, clearance 3 micron and groove angle 25° might be optimal. The effect of RPM with other conditions fixed is shown in Fig. 7, and the lift is almost linearly dependent on RPM.

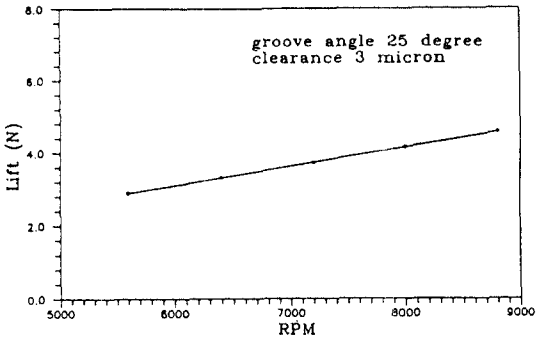

Fig. 7. Lift as a function of RPM.

4-2. Cases with Eccentricity

For the cases with eccentricity two-dimensional program explained in section 3 is used. In order to verify the code the pressure distributions obtained from one- and two-dimensional calculations are compared in Fig. 8, and there is very little discrepancies between two. In Fig. 9 the convergence characteristics of the two-dimensional calculation for the case of Fig. 8 is shown, and we note that a significant computing time is required for the error to reach the round off error range.

In Fig. 10 we show the pressure distribution for the case of groove angle 25°, clearance 3 micron and the eccentricity 1 micron. Although the picture looks somewhat confusing, we notice that there are fluctuating high and low pressure regions in both axial and circumferential directions. The highest peak is located around 0.018 in the circumferential direction and around 0.029 in the axial direction. The lowest is located around 0.028 in the circumferential direction and around 0.005 in the axial direction.

For better understanding, the pressure distribution for the similar case but without grooves is shown in Fig. 11. We can see an elongated high pressure region is generated just behind the circumferential location of the smallest spindle/sleeve gap and also an elongated low pressure region is generated a little behind the circumferential location of the biggest spindle/sleeve gap. Those are due the compression and suction behind and ahead, respectively, of the "flow stagnating converging-diverging nozzle". This

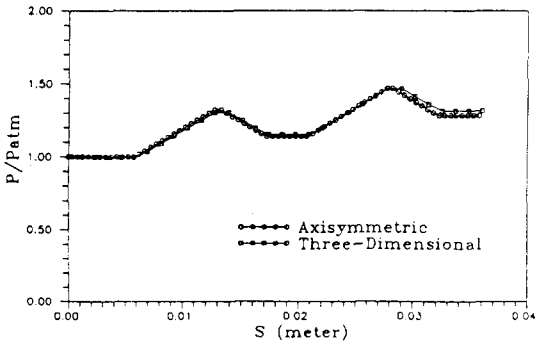

Fig. 8. Comparison of axisymmetric and two-dimensional calculations. Groove array is given in Fig. 2.

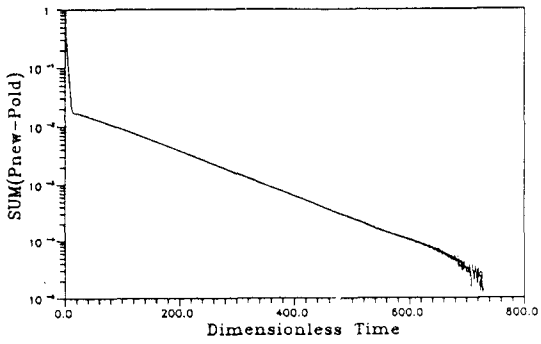

Fig. 9. A typical convergence characteristics of two-dimensional calculation.

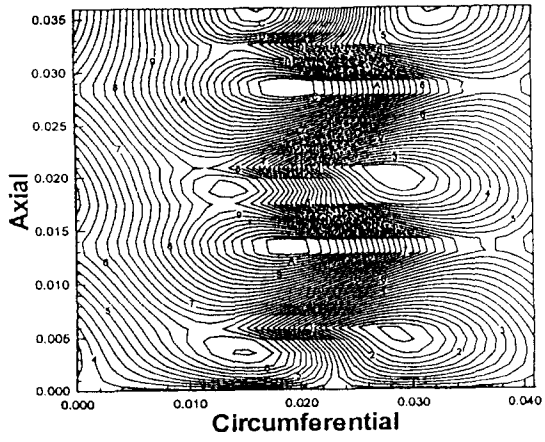

Fig. 10. Pressure distribution with 1 micron eccentricity with grooves given in Fig. 2.

phenomenon is consistent with well known facts from journal bearing problems. Now, recalling the pressure distribution in Fig. 8 (with grooves and

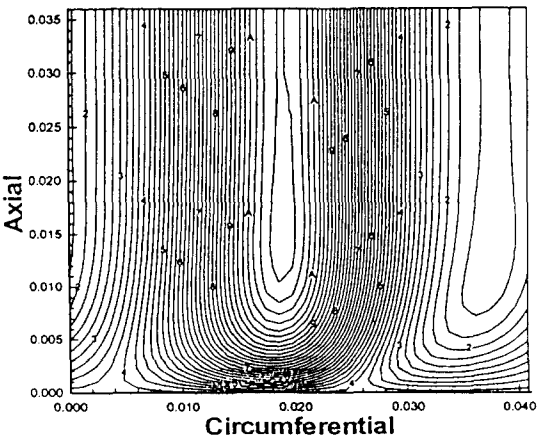

Fig. 11. Pressure distribution with 1 micron eccentricity without grooves.

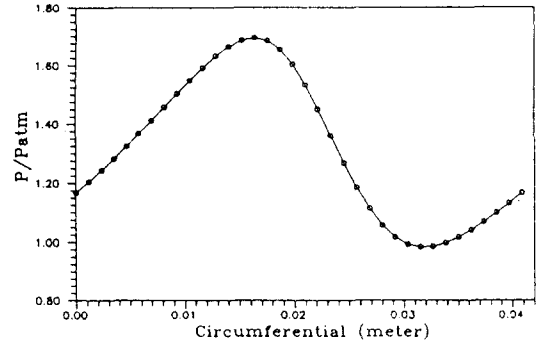

Fig. 12. Circumferential pressure distribution at the top.

without eccentricity) and superposing the pressure on the pressure given in Fig. 11 might give a similar pressure distribution given in Fig. 10. Ignoring differences possibly caused by nonlinear interaction between the effects of groove and eccentricity, we can understand the pressure obtained in Fig. 10 basically as a linear combination of those two effects.

In Fig. 12 the pressure at the top in the circumferential direction is shown. As we notice, since the pressure is mostly above the atmospheric pressure and, in the mean sense, is about the same magnitude as one in Fig. 8, we can expect a considerable lift force. However this type of pressure distribution causes tilting moment and the pressure given in Fig. 10 also causes unsymmetric force and moment on the sleeve, which in turn give effects on the sleeve's posture. Hence we believe a more careful investigation

on this problem is necessary including the information about the actual sleeve to be used.

5. Summary

Aiming at the development of rotor/spindle set operating at high speed (7200 RPM) and also providing a certain amount of lift force naturally generated by the air flow driven, problems associated with the design are considered. For the preliminary design, the pressure equation based on the narrow groove theory was solved by using a standard finite difference method. For cases with or without eccentricity one- and two-dimensional program are developed and their reliability is proved acceptable.

Based on the numerical results, pressure peaks, pressure distribution and lift force can be controlled by changing groove angle and the array of groove sets. we showed that the lift force is almost linearly dependent on the rotating speed and there exists an optimal groove angle for a certain amount of lift force although this value depends on the clearance.

If eccentricity is given, although the lift and the bearing stiffness seem sufficient in the mean sense, the pressure distribution becomes highly unsymmetric, so, in terms of sleeve's posture, further careful investigation should be carried out.

The performance of the manufactured prototype based on the proposed design looks acceptable and further validating experiment is underway.

6. References

1. Saito,S. and Tajima, K., "High-speed Laser Beam Printer," Hitachi Review, 183-186, 1984.
2. Sato, Y., Ono, K., "The optimum Groove Geometry for Spiral Groove Viscous Pumps," J. of Tribology, 409-414, 1990.
3. Tanaka, K. and Muraki, H., "Performance of Air-Lubricated Hydrodynamic Bearing Spindles for Laser Scanners," J. Tribology, 609-614, 1991.
4. Castelli, V. and Pirvics, J., "Review of numerical methods in gas bearing film analysis," J. Lub. Tech., 1968.
5. Kang, Kyung-Phil and Rhim, Yoon-Chul, "A study on the load characteristics of air-lubricated hydrodynamic herringbone-grooved journal bearing," J. of KSTLE, Vol.10, No.1, 27-34, 1994.
6. Kim, Sung-Gyun, Park, Sang-Shin and Han, Dong-Chul, "Analysis of the conical air bearings with two circumferential grooves," J. of KSTLE, Vol.10, No.1, 56-61, 1994.
7. Hsing, F.C., "Formulation of a Generalized Narrow Groove Theory for Spiral Grooved Viscous Pumps," J. Lub. Tech., 81-85, 1972.
8. Hsing, F.C., "Analytical Solutions for Incompressible Spiral Groove Viscous Pumps," J. Lub. Tech., 365-369, 1974.
9. Hsing, F.C. and Malanoski, S.B., "Mean free path effect spiral-grooved thrust bearings," J. Lub. Tech, Trans. ASME Series F, Vol.91, No.1, 1969.
10. Smalley, A.J., "The Narrow Groove Theory of Spiral Grooved Gas Bearings," J. Lub. Tech., 86-92, 1972.
11. Yih, C.S., Fluid Mechanics, McGraw-Hill, 1969.
12. Peyret, R. and Taylor, T.D., Computational Methods for Fluid Flow, Springer-Verlag, 1983.